SCIENCE CHINA
Chemistry

•COMMUNICATIONS•

https://doi.org/10.1007/s11426-019-9621-x

Temperature-induced Sn(II) supramolecular isomeric frameworks as promising heterogeneous catalysts for cyanosilylation of aldehydes

Kai Sheng[1,2†], Li-Ming Fan[3†], Xue-Fei Tian[1], Rakesh Kumar Gupta[1*], Linna Gao[4], Chen-Ho Tung[1] & Di Sun[1*]

[1]*Key Laboratory of Colloid and Interface Chemistry, Ministry of Education, School of Chemistry and Chemical Engineering, State Key Laboratory of Crystal Materials, Shandong University, Jinan 250100, China;*
[2]*School of Aeronautics, Shandong Jiaotong University, Jinan 250037, China;*
[3]*Department of Chemistry, College of Science, North University of China, Taiyuan 030051, China;*
[4]*College of Chemical and Environmental Engineering, Shandong University of Science and Technology, Qingdao 266590, China*

Received August 27, 2019; accepted September 20, 2019; published online December 11, 2019

Two novel Sn(II) supramolecular isomeric frameworks, with the identical formula of $\{(NH_2Me_2)_2[Sn(BDC)(SO_4)]\}_n$, Sn-CP-1-α (**1**) and Sn-CP-1-β (**2**) (H_2BDC=terephthalic acid) were synthesized under solvothermal condition and fully characterized by single crystal X-ray diffraction (SCXRD), Fourier transform infrared spectroscopy (FTIR), ultraviolet-visible spectroscopy (UV-Vis), elemental analyses, and thermogravimetric analysis (TGA). Interestingly, the structures of **1** and **2** are governed by the temperature of the reaction, suggesting a temperature-induced supramolecular isomerism. The supramolecular isomers are primarily caused by the different bridging alignments of $SO4^{2-}$. Compounds **1** and **2** display 2D layer and 3D framework with different topologies, non-interpenetrated 4^4-*sql* and two-fold interpenetrated 4-connected *dia* topology, respectively. Due to Lewis acid properties of coordinatively unsaturated Sn(II) sites in CPs, they have been utilized as heterogeneous catalyst for the cyanosilylation of aldehydes with an excellent conversion yield over 99% under solvent-free conditions.

supramolecular isomerism, Sn(II) coordination polymers, catalysis, cyanosilylation

Citation: Sheng K, Fan LM, Tian XF, Gupta RK, Gao L, Tung CH, Sun D. Temperature-induced Sn(II) supramolecular isomeric frameworks as promising heterogeneous catalysts for cyanosilylation of aldehydes. *Sci China Chem*, 2019, 62, https://doi.org/10.1007/s11426-019-9621-x

The current research interests in coordination polymers (CPs) are due to their fascinating architectures and miscellaneous applications, including gas storage, luminescence, catalysts, sensors, and drug delivery [1,2]. The real applications of CPs are directly associated with their crystalline properties of materials [3,4]. Therefore, the design and synthesis of desired CPs with predictable metal-organic connectivity is still challenging due to supramolecular isomerism [5,6]. Supramolecular isomerism or polymorphism refers to the existence of more than one crystal structure that has the same chemical composition and building blocks [7,8]. Polymorphism in CPs are governed by many key factors such as reaction medium, temperature, counter ions, pH values, and solvent [9–12]. Among them, the effect of temperature is one of the most significant variables [9,13]. In the recent past, majority of the supramolecular isomeric CPs are available either on transition metals or lanthanides [7–12]. It should be noted that polymorphism in main group metal complexes, particularly tin complexes are barely explored. To the best of our knowledge, only a few examples of polymorphism in Sn(IV) complexes are available, but the

---

†These authors contributed equally to this work.
*Corresponding authors (email: rkg@sdu.edu.cn; dsun@sdu.edu.cn)

examples of temperature-induced polymorphism in Sn(II) CPs are not described so far [14–16].

On the other hand, cyanosilylation of carbonyl compounds with trimethylsilyl cyanide (TMSCN) is an effective method to synthesize cyanohydrins, which are important precursors for the synthesis of natural and pharmaceutical compounds, in presence of Lewis acid catalyst [17,18]. In this context, numerous metal complexes and coordination polymers have been studied as homogeneous catalysts; however, heterogeneous catalysts are limited [19–23]. Therefore, the design and development of heterogeneous catalyst, which is inexpensive, solvent free and easy to handle, are highly desirable. The large size and stereo chemical effect of the lone pair of tin endow them Lewis acid characteristics as a consequence superior catalytic properties [15,24,25]. To our best knowledge, the application of a Sn(II) complex as a heterogeneous catalyst for cyanosilylation of aldehydes under solvent-free conditions has not been testified.

Hence, terephthalic acid ligand has been selected to develop some supramolecular Sn(II) isomeric CPs with excellent heterogeneous catalytic activity. Remarkably, Jacobson *et al.* [26], have synthesized some tin terephthalates metal complexes $A_2Sn_2(BDC)_3(H_2O)_x$, A=Li, Na, K, Rb, Cs, under hydrothermal condition at 200 °C for 6 d in the presence of alkali metal hydroxides. Further, a 3D framework structure of $Sn_3O(BDC)_2$ was reported by the same group at 180 °C for 24 h [27].

All above discussions clearly indicated that the Sn(II) CPs are still quite rare in CPs field, compared to other metal congeners. Keeping all these considerations and also inspired by our previous work [28], we have successfully isolated two supramolecular isomeric Sn(II) CPs, with exactly the same chemical composition of $\{(NH_2Me_2)_2[Sn(BDC)(SO_4)]\}_n$ by adjusting the reaction temperature. Compounds **1** and **2** show 2D layer and 3D framework with different topologies, non-interpenetrated 4^4-*sql* and two-fold interpenetrated 4-connected *dia* network, respectively. Furthermore, heterogeneous catalytic activities have been established towards the cyanosilylation of aldehydes with TMSCN in detail.

Compounds **1** and **2** were synthesized under solvothermal condition by the reaction of H_2BDC and $SnSO_4$ at different temperatures (180 °C for **1**; 150 °C for **2**) using similar concentration of reactants (Scheme 1). **1** and **2** have the identical composition, but different crystal structures signifying temperature-dependent supramolecular isomerism, which has been supported by single-crystal X-ray diffraction (SCXRD) analysis. The morphology of the crystals appearance under a microscope is depicted in Scheme 1.

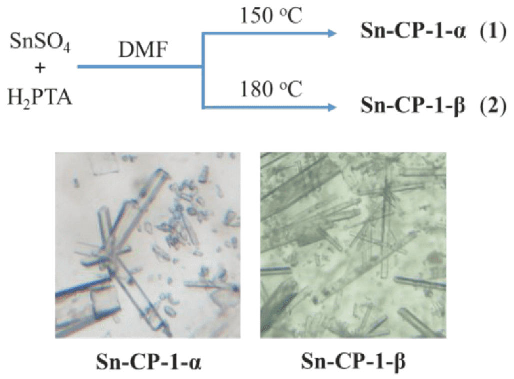

Sn-CP-1-α **Sn-CP-1-β**

Scheme 1 Schematic illustration of synthesis of isomers **1** and **2**, and the crystal images under a microscope (color online).

Single crystal X-ray diffraction analyses show that **1** and **2** crystallize in the monoclinic $P2_1/n$ and orthorhombic *Pbca* space groups, respectively (Tables S1 and S2, Supporting Information online). Asymmetric units are similar, consist of one Sn(II) ion, two half BDC^{2-} ligand, one SO_4^{2-} anion, and two $NH_2Me_2^+$ cations (Figure 1(a, b)). Each Sn(II) ion was surrounded by four O atoms from two different BDC^{2-} ligands and two SO_4^{2-} anions, forming the distorted $\{SnO_4\}$ tetrahedrons which can be better described as a seesaw structure with τ_4=0.88 for **1** and τ_4=0.84 for **2** [29]. The linear O5–Sn1–O6 forms the plank and O1–Sn1–O3 forms the pivot in **1**. The O5–Sn1–O6 and O1–Sn1–O3 planes are nearly perpendicular to each other with a dihedral angle (DA) of around 88.3°. Similarly, in compound **2**, O5–Sn1–O8 and O2–Sn1–O3 forms the plank and pivot, respectively. The DA of around 89.3° was observed with the nearly perpendicular O5–Sn1–O6 and O1–Sn1–O3 planes. The Sn–O bond lengths span from 2.165(3) Å (Sn1–O1) to 2.502(5) Å (Sn1–O6A) for **1** (Figure 1(c)), and 2.163(4) Å (Sn1–O3) to 2.660(5) Å (Sn1–O8C) for **2** (Figure 1(d)), respectively, which are comparable with the earlier reports [26,27,30] (Tables S3 and S4) (symmetry codes: A: 1+*x*, *y*, *z*; C: 0.5−*x*, −0.5+*y*, *z*).

Although, the asymmetric unit is similar, a minor difference leads to huge structural differences. In the construction of **1** and **2**, carboxyl groups of BDC^{2-} ligands all adopt monodentate coordination modes and act as bridging linkers to connect the Sn(II) ions, giving 1D $[Sn(BDC)]_n$ chains with the separated Sn···Sn distances being 11.39 and 11.44 Å for **1**, and 11.34 and 11.42 Å for **2**, respectively. The DA originated by the two BDC rings is 10.9° for **1**, and 13.2° for **2**.

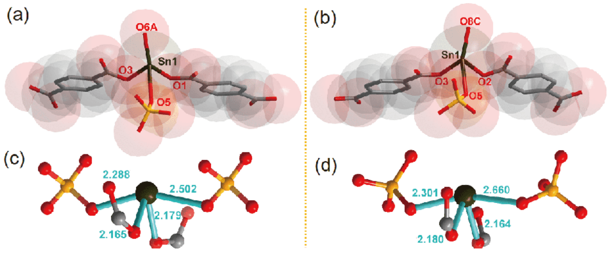

Figure 1 The asymmetric units of **1** (a) and **2** (b); the coordination environments of Sn(II) centres of **1** (c) and **2** (d). Colour code: Sn, brownish green; S, yellow; O, red; C, grey (color online).

The Sn···Sn···Sn angles along the linear axis of BDC^{2-} ligand was found to be 101.42° for **1** and 102.62° for **2**, respectively. Meanwhile, the SO_4^{2-} occupied the pole position to bridge the Sn(II) ions to form 1D $[Sn(SO_4)]_n$ chain with Sn···Sn distances being 6.83 Å for **1**, and 6.58 Å for **2**, respectively. Sharing the Sn(II) ions, the wavy 2D layer of **1** was constructed (Figure 2(a, c)), which can be simplified into a 4^4-*sql* sheet (Figure 3(a)). While, 3D two-fold interpenetrated 4-connected uninodal networks was constructed for **2** (Figure 2(b, d)), which can be simplified as a *dia* framework with Schläfli symbol $\{6^6\}$ and extended point symbol $[6_2.6_2.6_2.6_2.6_2.6_2.]$. Based on interpenetration classification and nomenclature, the type of interpenetration in **2** belongs to class IIa, *Z*=2, which suggests two identical interpenetrated nets are generated by means of space group interpenetration symmetry elements, here are 2-fold axes along crystallographic *b* and *c* directions, and no interpenetrating translations are allowed in this kind of interpenetration (Figure 3(b)) [31].

The 2D layered non-interpenetrated sheet of **1** and two-fold interpenetrated 3D framework of **2** are true supramolecular isomers because they have different network structures but exactly the same chemical compositions. The differences in their networks are associated with the alteration in their coordination environment. The key difference between the structures of these isomers is the bridging orientation of the SO_4^{2-} around the Sn(II) centers. In **1**, the SO_4^{2-} ions show a uniform orientation, wherein each SO_4^{2-} binds with another metal center with the bond angles of Sn1–O5–S1, 124.51°, Sn1–O6–S1, 120.45° and O5–S1–O6, 105.40° for **1** (Figure 2(a)). However, in **2**, SO_4^{2-} ions adopt alternate arrangement on binding two further metal centers (Figure 2(b)) with the bond angles of Sn1–O5–S1, 120.45°; Sn1–O5–S1, 115.56°; and O5–S1–O6, 111.67°. The DAs of 46.51° and 30.21° were observed with the plane defined by S1–O5–Sn1 and S1–O6–Sn1, **1**; and S1–O5–Sn1 and S1–O8–Sn1, **2**. The plane generated through Sn1–O5–S1–O6 is parallel to each other in **1**, whereas in **2**, torsion angle is 17.33°. The Sn···Sn···Sn angles of 180° in **1** cause more regular geometry and a 2D layer sheet is formed finally, along SO_4^{2-} axis. Whereas, in **2**, Sn···Sn···Sn angle of 169.61° causes more distortion from the regular geometry and a 3D structure is generated finally. These geometric differences together result into the formation of 2D layer non-interpenetrated sheet in **1**, and two-fold interpenetrated 3D framework in **2**. Thus the bridging orientations of the SO_4^{2-} cause different connectivity between the metal centers and thus lead to the formation of true supramolecular isomers **1** and **2**.

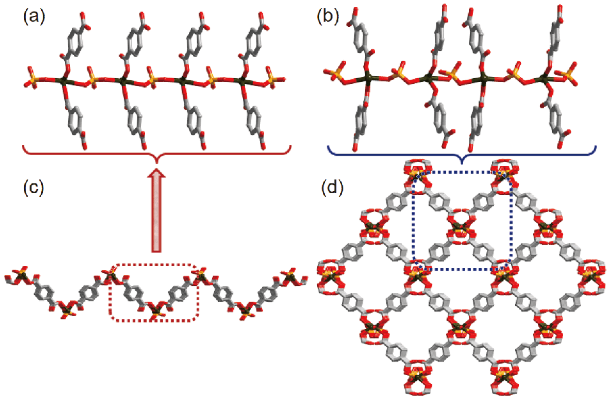

Figure 2 The alignment of SO_4^{2-} (a) 2D layered non-interpenetrated structure of **1** (c); alternate arrangement of SO_4^{2-} connecting to another metal centers (b) two-fold interpenetrated 3D structure of **2** (d). Colour code: Sn, brownish green; S, yellow; O, red; C, grey (color online).

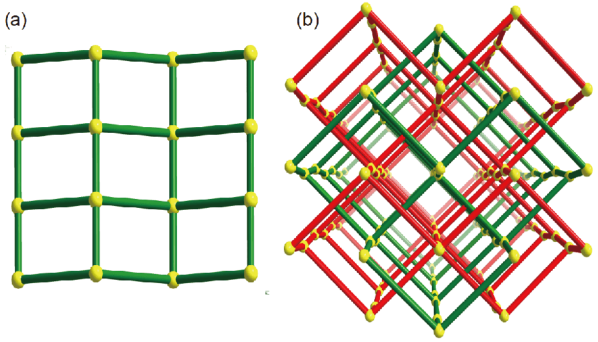

Figure 3 (a) The 4-connected *sql* sheet for **1** and (b) the two-fold interpenetrated 4-connected *dia* net for **2** (color online).

The UV-Vis absorption spectra of **1** and **2** were measured in the solid state (Figure S1, Supporting Information online) using diffusion-reflection mode. The absorption maxima of **1** and **2** exhibited at 308 and 312 nm respectively in the ultraviolet region. These absorption bands are assigned to *s-p* transitions of Sn(II) systems [32,33].

Thermogravimetric analysis (TGA) was carried out to check the thermal stabilities of both Sn(II) CPs. The features of thermal stability are illustrated in Figure S2. Both compounds are stable up to ca. 180 °C, and exhibit similar weight loss pattern. For **1**, the first major weight loss (35.2%) occurred in the range of 180–320 °C, attributed to the removal of organic ligand BDC (34.8%). Similarly, **2** also showed a weight loss of 34.5% consistent to the loss of organic ligand (34.8%) in the temperature range 180–350 °C. Then, the weight loss above aforesaid temperature leads to the loss of NH_2Me_2, SO_4, and thermally stable final product corresponding SnO. The TGA analyses show that all compounds are thermally stable and can meet the conditions for catalytic reactions as discussed below.

Based on the single-crystal structures of two Sn(II) CPs, both compounds show coordinatively unsaturated Sn^{II} centers in frameworks, which encourages us to evaluate their activity as heterogeneous catalysts towards Lewis acid promoted reactions. Here, we choose a typical reaction for testing Lewis acidity catalysis: cyanosilylation of aldehyde, since the cyanosilylation of aldehydes is an efficient route for preparation of cyanohydrins, which are key intermediates in the synthesis of various biologically active molecules [17,18]. Firstly, we use solvent-free cyanosilylation of benzaldehyde as a model reaction to explore the activity of **1** and **2**.

Figure 4 shows the kinetic reaction profile (conversion versus time) of the reaction between benzaldehyde and TMSCN. The values of conversion based on ^{1}H NMR integrations and their corresponding ^{1}H NMR spectra are shown in Table S5 and Figures S4–S21, respectively. The plots reveal that both **1** and **2** are excellent catalysts for cyanosilylation reaction. Especially, **2** shows better catalytic activity than **1** with the conversion up to more than 99%, whereas that of **1** reaches only 96% under the same catalytic reaction conditions (1 mol% loading and room temperature). Such catalysis reaction kinetic behaviors were also supported by time-dependent infrared spectra (Figure S22).

Furthermore, aldehyde substrates with a larger conjugated system (Table 1) are further examined by using **2** as the catalyst. The corresponding ^{1}H NMR spectra are shown in Figures S23–S31. The complete conversion of *o*-Me-, *m*-Me- and *p*-Me-substituted benzaldehydes can be achieved within 2 h at room temperature (entries 3–5). With the *p*-*t*Bu-substituted benzaldehyde, the reaction is slightly slower and lower conversion (entry 6). For bulkier naphthaldehyde, only a 47% conversion is given in 2 h and it can also achieve full conversion when the reaction time extends to 5 h (entry 7). This steric hindrance effect indicates the bulkier substrates are more difficult to access the catalytic sites [34,35]. The fluorine substituted substrate can also be tolerated (entry 8). For ketones, however, the reaction is much slower owing to the lower activity of ketones than aldehydes (entry 9). The control experiment, without the catalyst, shows little conversion of only 3% under the same conditions (entry 10).

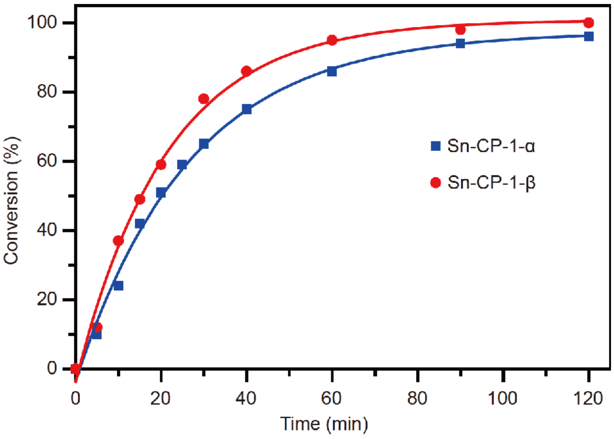

Figure 4 The kinetic reaction profile of the cyanosilylation catalysed by 1 mol% of **1** and **2** (based on ^{1}H NMR integrations) (color online).

In order to understand the heterogeneous catalytic nature of the reaction, the catalyst is separated from the reaction after 20 min by centrifugation and filtration. The filtrate is allowed to stir under the same conditions for additional 100 min. No significant increase of conversion can be observed (Figure S32), demonstrating the heterogeneous nature of the catalysis. Moreover, the solid catalyst has been collected after centrifugation, washed with chloroform and methanol and dried at 65 °C for 5 h for recovery. The recycling test shows that it can be reused at least for three cycles with slight loss of activity (Figure S33).

In conclusion, two novel Sn(II) supramolecular isomeric frameworks, Sn-CP-1-α and Sn-CP-1-β have been synthesized and fully characterized. Interestingly, the structures of **1** and **2** are dependent on the temperature of the reaction at

Table 1 Results of cyanosilylation of varied aromatic aldehydes/ketone in the presentence of Sn-CP-1-α orSn-CP-1-βat room temperature a)

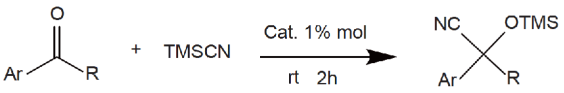

Entry	Catalyst	Ar	R	Conversion b) (%)	TOF c) (h^{-1})
1	**1**	Ph	H	96	48
2	**2**	Ph	H	>99	49.5
3	**2**	*o*-MeC_6H_4	H	>99	49.5
4	**2**	*m*-MeC_6H_4	H	>99	49.5
5	**2**	*p*-MeC_6H_4	H	>99	49.5
6	**2**	*p*-*t*BuC_6H_4	H	95	47.5
7	**2**	1-Naphtyhyl	H	47 (99) d)	23.5
8	**2**	*o*-FC_6H_4	H	>99	49.5
9	**2**	Ph	Me	5	2.5
10	No catalyst	Ph	H	3	1.5

a) General reaction conditions: aldehyde/ketone (1 mmol), TMSCN (1.2 mmol), catalyst **1** or **2** (0.01 mmol), room temperature, 2 h. b) The conversions are calculated based on ^{1}H NMR integration of the product peaks in comparison to those of the aldehyde/ketone. c) TOFs are calculated as moles of product formed per hour and per mole of Lewis acidic active site. d) Reaction time: 5 h.

180 and 150 °C, respectively. Compounds **1** and **2** display wavy 2D layer and 3D framework with different topologies, non-interpenetrated 4^4-*sql* and two-fold interpenetrated 4-connected *dia* network. Furthermore, both of them show excellent heterogeneous catalytic activity towards solvent free cyanosilylation of various aldehydes to the corresponding cyanohydrins in excellent yields as high as 99% with 1 mol% (Sn-CP-1-β) of catalyst at room temperature for 2 h. The reaction kinetic behaviors were supported by time dependent infrared and ^{1}H NMR spectra. These are the first example of coordinatively unsaturated supramolecular isomeric Sn(II) CPs with excellent heterogeneous catalytic activity towards cyanosilylation reactions of aldehydes.

Acknowledgements This work was supported by the National Natural Science Foundation of China (21822107, 21571115, 21827801, 21671172), the Natural Science Foundation of Shandong Province (JQ201803, ZR2017MB061, ZR2017ZF003), the Taishan Scholar Project of Shandong Province of China (tsqn201812003), the Qilu Youth Scholar Funding of Shandong University and the Fundamental Research Funds of Shandong University (104.205.2.5), and the State Key Laboratory of Pollution Control and Resource Reuse Foundation (PCRRF18019).

Conflict of interest The authors declare that they have no conflict of interest.

Supporting information The supporting information is available online at http://chem.scichina.com and http://link.springer.com/journal/11426. The supporting materials are published as submitted, without typesetting or editing. The responsibility for scientific accuracy and content remains entirely with the authors.

1 Cui Y, Li B, He H, Zhou W, Chen B, Qian G. *Acc Chem Res*, 2016, 49: 483–493
2 Li B, Wen HM, Cui Y, Zhou W, Qian G, Chen B. *Adv Mater*, 2016, 28: 8819–8860
3 Zhou HC, Long JR, Yaghi OM. *Chem Rev*, 2012, 112: 673–674
4 Tan YX, Wang F, Zhang J. *Chem Soc Rev*, 2018, 47: 2130–2144
5 Zhang JP, Huang XC, Chen XM. *Chem Soc Rev*, 2009, 38: 2385–2396
6 Moulton B, Zaworotko MJ. *Chem Rev*, 2001, 101: 1629–1658
7 Robin AY, Fromm KM. *Coord Chem Rev*, 2006, 250: 2127–2157
8 Aulakh D, Varghese JR, Wriedt M. *Inorg Chem*, 2015, 54: 8679–8684
9 Cheetham AK, Rao CNR, Feller RK. *Chem Commun*, 2006, 216: 4780–4795
10 Hao ZM, Zhang XM. *Cryst Growth Des*, 2007, 7: 64–68
11 Masaoka S, Tanaka D, Nakanishi Y, Kitagawa S. *Angew Chem Int Ed*, 2004, 43: 2530–2534
12 Fang HC, Ge YY, Jia HY, Li SS, Sun F, Zhang LG, Cai YP. *CrystEngComm*, 2011, 13: 67–71
13 Dikhtiarenko A, Serra-Crespo P, Castellanos S, Pustovarenko A, Mendoza-Meroño R, García-Granda S, Gascon J. *Cryst Growth Des*, 2016, 16: 5636–5645
14 Kloskowska M, Konitz A, Wojnowski W, Becker B. *Z Anorg Allg Chem*, 2006, 632: 2424–2428
15 Karmakar A, Hazra S, Rúbio GMDM, Guedes da Silva MFC, Pombeiro AJL. *New J Chem*, 2018, 42: 17513–17523
16 Chen GH, He YP, Zhang SH, Liang FP, Zhang L, Zhang J. *Inorg Chem*, 2019, 58: 12521–12525
17 Gustafsson M, Bartoszewicz A, Martin-Matute B, Sun J, Grins J, Zhao T, Li Z, Zhu G, Zou X. *Chem Mater*, 2010, 22: 3316–3322
18 Dang D, Wu P, He C, Xie Z, Duan C. *J Am Chem Soc*, 2010, 132: 14321–14323
19 Liu J, Chen L, Cui H, Zhang J, Zhang L, Su CY. *Chem Soc Rev*, 2014, 43: 6011–6061
20 García-García P, Müller M, Corma A. *Chem Sci*, 2014, 5: 2979–3007
21 Kurono N, Ohkuma T. *ACS Catal*, 2016, 6: 989–1023
22 He H, Ma H, Sun D, Zhang L, Wang R, Sun D. *Cryst Growth Des*, 2013, 13: 3154–3161
23 Du JJ, Zhang X, Zhou XP, Li D. *Inorg Chem Front*, 2018, 5: 2772–2776
24 Evans DA, MacMillan DWC, Campos KR. *J Am Chem Soc*, 1997, 119: 10859–10860
25 Samuel PP, Shylesh S, Singh AP. *J Mol Catal A-Chem*, 2007, 266: 11–20
26 Wang X, Liu L, Makarenko T, Jacobson AJ. *Cryst Growth Des*, 2010, 10: 1960–1965
27 Wang X, Liu L, Makarenko T, Jacobson AJ. *Cryst Growth Des*, 2010, 10: 3752–3756
28 Zhao YQ, Yu K, Wang LW, Wang Y, Wang XP, Sun D. *Inorg Chem*, 2014, 53: 11046–11050
29 Yang L, Powell DR, Houser RP. *Dalton Trans*, 2007, 60: 955–964
30 Li W, Du D, Liu S, Zhu C, Sakho AM, Zhu D, Xu L. *J Organomet Chem*, 2010, 695: 2153–2159
31 Blatov VA, Carlucci L, Ciani G, Proserpio DM. *CrystEngComm*, 2004, 6: 377–395
32 Grusenmeyer TA, King AW, Mague JT, Rack JJ, Schmehl RH. *Dalton Trans*, 2014, 43: 17754–17765
33 Vogler A, Paukner A, Kunkely H. *Coord Chem Rev*, 1990, 97: 285–297
34 Zhu C, Xia Q, Chen X, Liu Y, Du X, Cui Y. *ACS Catal*, 2016, 6: 7590–7596
35 Wang XP, Zhao YQ, Jagličić Z, Wang SN, Lin SJ, Li XY, Sun D. *Dalton Trans*, 2015, 44: 11013–11020